Analysis and Compensation of Phase Noise in mm-Wave OFDM ARoF Systems for Beyond 5G

Analysis and Compensation of Phase Noise in mm-Wave OFDM ARoF Systems for Beyond 5G

Javier Pérez Santacruz, Simon Rommel, *Member, IEEE, Member, OSA,* Ulf Johannsen, *Member, IEEE,* Antonio Jurado-Navas, *Member, OSA,* and Idelfonso Tafur Monroy, *Senior Member, IEEE,*

***Abstract*—Fifth-generation mobile networks (5G) are the solution for the demanding mobile traffic requirements, providing technologies that fulfill the requisites of different type of services. The utilization of the millimeter-wave (mm-wave) band is the straightforward technique to achieve high bit rates. Moreover, analog radio-over-fiber (ARoF) brings outstanding benefits such as low cost, low power consumption, and high spectral efficiency, among others. Thereby, mm-wave ARoF is a strong candidate to pave the way for common public radio interface (CPRI) in the fronthaul for the future 5G architecture. As orthogonal frequency-division multiplexing (OFDM) is the adopted waveform in the 5G standard, it should be also utilized in mm-wave ARoF systems for 5G. However, phase noise is one of the most degrading factors in mm-wave OFDM ARoF systems. Therefore, in this work, an analysis of the phase noise is carried out through an experimental setup up. The configuration of this setup enables to gradually modify the final phase noise level of the system. Furthermore, an original and novel algorithm to compensate the phase noise in OFDM receivers is proposed. The performance of this algorithm is experimentally evaluated through the setup for different phase noise levels and different subcarrier spacings. The obtained results show the effectiveness of the proposed algorithm under those conditions, highlighting the viability of mm-wave OFDM ARoF for 5G and beyond.**

***Index Terms*—5G, phase noise, ARoF, OFDM, mm-wave.**

I. Introduction

MOBILE network data has exponentially grown in the last years. The fifth-generation (5G) of mobile networks is the adopted solution for this increasing traffic trend. 5G will support a huge enhancement in terms of capacity, bit rate, latency, reliability, energy efficiency, and number of connected devices [1]. Many technologies have appeared to fulfill these demanding requirements [2]. Thus, to achieve high bit rates, the need for achieving higher data rates leads is forcing operators to move toward high-frequency bands, being the millimeter-wave (mm-wave) domain a very promising one due to its inherent bandwidth. Transmitting signals at mm-wave frequencies implies high free-space path loss (FSPL) and, for that reason, the area of mm-wave cells does not exceed 200 m [3]. Therefore, a larger number of mm-wave cells, compared to the current mobile network, are required to cover the same surface.

Since centralized radio access network (C-RAN) implies higher flexibility, lower latency, and lower power consumption than distributed radio access network (D-RAN), this centralized architecture is a more preferable solution for 5G [4]. Digital radio-over-fiber (DRoF) is the adopted technology in common public radio interface (CPRI) to develop C-RAN in the mobile network. However, CPRI requires constant bitrate signals and implies sampling rates of hundred of Gbit/s. Thereby, DRoF is clearly not a scalable solution for the future mm-wave 5G architecture [5]. On the other hand, analog radio-over-fiber (ARoF) reduces the complexity, cost, and latency in the remote unit (RU), avoiding the high demanding analog-to-digital converters (ADCs) and digital-to-analog converters (DACs) used in DRoF [4]. Therefore, C-RAN architecture employing ARoF is a suitable solution for the mm-wave 5G fronthaul since it brings attractive benefits such as low latency, low cost, high scalability, high spectral efficiency, and low power consumption [6]–[8].

Orthogonal frequency-division multiplexing (OFDM) is the 5G waveform standardized by 3rd Generation Partnership Project (3GPP) [9]. In the new radio (NR), 5G defines different numerologies for OFDM [9] associated to subcarrier spacing values from 15 to 240 kHz. OFDM offers solid wireless communications due to its robustness to frequency selective channels, high spectral efficiency, low out-of-band (OOB) emissions, and efficient multiple-input and multiple output (MIMO) integration [10], [11]. Accordingly, mm-wave cells over ARoF with OFDM is a strong candidate to be part of the beyond 5G architecture. However, the phase noise has been demonstrated to be one of the major performance limiting factor in OFDM mm-wave ARoF systems because of the relatively low subcarrier spacing used in 5G [5], [12].

Strategies to compensate the phase noise degradations have already been analyzed and evaluated in OFDM mm-wave ARoF systems: thus, the phase noise is mitigated by hardware in [13], [14]; and dispersion-induced phase noise (DPN) included by the chromatic dispersion of the fiber is compensated for long fiber distance in [15], [16]. Moreover, the impact of phase noise has been studied and analyzed in [12] for OFDM signals with different numerologies. Other modulation formats, such as universal filtered-OFDM (UF-OFDM), have also been

Manuscript received September ??, 2020; revised MMM DD, 2020, accepted MMM DD, YYYY. This work was partially supported by the ITN 5G STEP-FWD and blueSPACE projects which has received funding from the European Union's Horizon2020 research and innovation program under grant agreements No. 722429 and 762055.

J. Pérez Santacruz, S. Rommel and I. Tafur Monroy are with the Institute for Photonic Integration, Eindhoven University of Technology, 5600 MB Eindhoven, The Netherlands (e-mail: j.perez.santacruz@tue.nl).

U. Johannsen is with the Centre for Wireless Technology, Eindhoven University of Technology, 5600 MB Eindhoven, The Netherlands.

A. Jurado-Navas is with the Communication Engineering Department, University of Málaga, 29071 Málaga, Spain.

Color versions of one or more of the figures in this paper are available online at http://ieeexplore.ieee.org.

Digital Object Identifier 10.1109/JLT.2020.XXXXXX

evaluated in terms of phase noise in this type of systems [17], [18]. Nevertheless, the performance of a technique to mitigate the phase noise for different phase noise levels and different numerologies in OFDM mm-wave ARoF scenarios has not yet been realized. For this reason, in this work, a novel OFDM algorithm to compensate phase noise is proposed and explained. Next, the mm-wave ARoF phase noise is studied and analyzed in an experimental setup at 25 GHz (K-band). This setup allows to gradually increase the phase noise level. Then, the OFDM performance is experimentally evaluated under different phase noise conditions and for all 5G numerologies. The proposed algorithm is used to enhance the performance of the received OFDM signals. The experimental results prove that the proposed OFDM receiver allows to achieve 5G requirements for different phase noise levels and different subcarrier spacings.

This manuscript is organized as follows: Section II describes the fundamentals of the proposed OFDM algorithm to mitigate the phase noise. Section III explains the employed ARoF setup to progressively increment the phase noise. Section IV studies the phase noise in the proposed ARoF scheme. Section V discusses the obtained results. Finally, Section VI presents some concluding remarks.

II. Proposed Algorithm to Compensate the Phase Noise in OFDM Systems

Phase noise is one of the major issues in OFDM systems. This impairment introduces a twofold degradation in the transmitted OFDM signal [15]: first, a common phase error (CPE), which affects to all the subcarriers similarly, can be compensated with the channel equalizer; and, second, an inter-carrier interference (ICI), deteriorating the subcarriers asymmetrically. Therefore, an additional method has to be performed in the OFDM receiver to compensate the ICI introduced by the phase noise. Furthermore, since phase noise degrades the orthogonality of the subcarriers in each OFDM symbol, the ICI level added by the phase noise is proportional to the OFDM symbol duration. The subcarrier spacing is inversely proportional to the symbol duration in OFDM systems. Thus, the subcarrier spacing is a relevant OFDM parameter that determines the ICI intensity introduced by the phase noise.

In this work, a novel algorithm to compensate the ICI induced by the phase noise in OFDM systems is presented and explained. This section is structured as follows: first, the fundamentals of the proposed algorithm are shown. Then, the keys to achieve high performance in this algorithm are detailed. Finally, some complexity and latency considerations about the algorithm are expounded.

A. Fundamentals of the algorithm

The classical block diagram for an OFDM transmitter is represented in Fig. 1 (a), where the process sequence is as follows: the flow of bits is mapped into the constellation symbols through the modulator; then, the inverse fast Fourier transform (IFFT) is performed; and, finally, the cyclic prefix (CP) is added to each OFDM symbol. In addition, the typical system

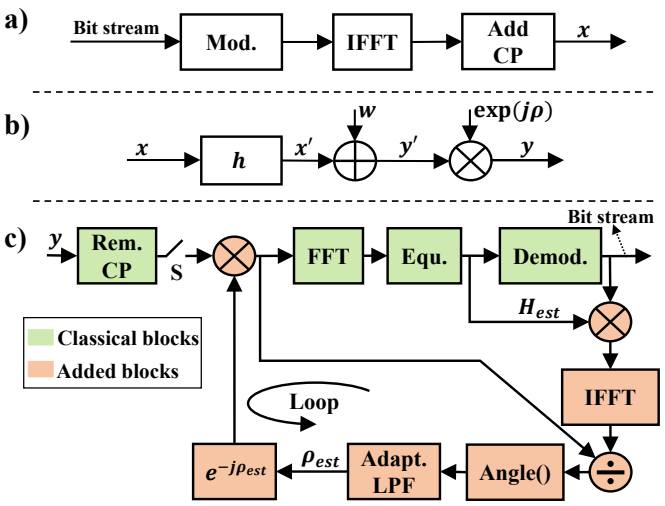

Figure 1. (a) Classical OFDM transmitter. (b) Phase noise channel model. (c) Block diagram of the proposed algorithm to compensate the phase noise in OFDM receivers (the switch S turns off after the first iteration).

model of a phase noise channel is shown in Fig. 1 (b) [19]. There, the transmitted signal x is convolved with the channel response h, obtaining x'. Then, the additive white Gaussian noise (AWGN) w is included, to obtain y'. The output signal y of the system model is generated by multiplying y' with the complex exponential of the phase noise ($\exp(-j\rho)$). Lastly, the block diagram of the proposed algorithm is shown in Fig. 1 (c). This algorithm is based on re-constructing the transmitted OFDM signal x in the time-domain. Then, this reconstructed signal is used as reference to estimate the phase noise. The only assumption required by the algorithm is that the phase noise spectrum behaves as a low-pass signal. Since phase noise follows a Wiener process in most communication scenarios [20], the low-pass nature assumption for phase noise is adequate for the majority of the mm-wave ARoF systems. An algorithm based on this assumption and strategy to estimate and compensate the phase noise is also used in [19], [21], [22]. This type of algorithms performs better when the channel is mainly dominated by the phase noise.

The block diagram of Fig. 1 (c) is structured in two parts: one part is compounded by the classical blocks in an OFDM receiver; the second part constitutes the additional blocks to estimate and compensate the phase noise. Regarding the first part, the classical OFDM receiver sequence is formed by the next constitutive elements: an initial one for removing the CP of each OFDM symbol; then, the fast Fourier transform (FFT) can be performed to move into the frequency-domain; next, the channel frequency response is estimated using the distributed pilot subcarriers and compensating the remaining subcarriers with this estimation; and, finally, the demodulation of the equalized symbols is accomplished according to the constellation used in the transmitter.

After the demodulation block, the additional elements to estimate and compensate the phase noise start. First, the demodulated symbols are multiplied by the estimated channel frequency response that is obtained in the equalizer block. Then, the resulting signal passes to the time-domain by per-

forming an IFFT. In this way, an estimation of the transmitted time-domain OFDM signal filtered by the channel response (x') is achieved. If both the demodulation procedure is error-free and the channel estimation error is negligible, such that the estimated time-domain signal becomes x'.

After the IFFT process, the estimated time-domain transmitted signal is divided by the received signal. Next, the angle of this division is calculated. Hence, a first estimation of the phase noise is accomplished. If the received signal only suffers the adverse effects of phase noise and of multipath channel degradations; and if there is no errors in the estimation of x', then no differences are appreciated between the initial estimation and the real phase noise. However, degradations in the received signal cause errors in the demodulation process and, thus, in both the phase noise and x' estimations. A way to enhance the phase noise estimate consists of filtering it according to the spectral shape of the phase noise. Then, in order to reduce the error in the estimation, the initial phase noise estimate is filtered. Next, the received signal is multiplied by the complex exponential of the inverse of the estimated phase noise ($\exp(-j\rho_{est})$). In this respect, the estimated phase noise is compensated in the received signal. Finally, the FFT, the channel equalizer, and the demodulator processes are performed again.

The proposed algorithm can be used iteratively to enhance the estimate of the phase noise and its compensation in each iteration. The first iteration contains more errors in the demodulation process than subsequent iterations because the phase noise was not compensated previously. In the second iteration, the phase noise is compensated by using the phase noise estimate from the first iteration before the demodulation and, thus, fewer errors appear in the demodulation process than in the previous iteration. Consequently, since the re-built time-domain signal is closer to x', the phase noise estimate enhances in the second iteration. Subsequent iterations calculate and compensate the residual phase noise that was not estimated in the previous iterations. Therefore, the number of errors due to the phase noise decrease with the number of iterations of this algorithm because the phase noise compensation is improved in each iteration.

This iterative process is applied on all subcarriers. Since the null subcarriers in the edge of the OFDM band are known in the receiver, the equalization and demodulation processes do not need to process these subcarriers in the algorithm, considering them null values. Therefore, the multiplication between the estimation of the channel (H_{est}) with the demodulated symbols includes only the active subcarriers. For the remaining added blocks of the algorithm, all subcarriers are involved in the process.

An additional block can be added after the demodulator block to decide when to leave the algorithm loop. This decision is based on an estimate of the signal-to-interference-plus-noise ratio (SINR) in the current iteration. Two parameters are evaluated for the aforementioned decision: an SINR threshold and an SINR step, that expresses the SINR improvement between the current iteration and the previous one. The algorithm loop can be finished when the SINR estimate is above the threshold or when the SINR step falls below a predefined limit value. In this way, infinite loops and unnecessary iterations can be avoided.

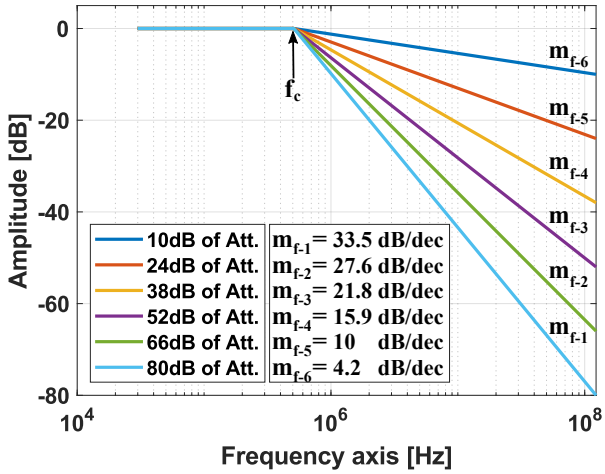

Figure 2. Example of an adaptive low-pass filter design for the proposed algorithm.

B. Filter design strategies

The low-pass filter (LPF) block plays a crucial role in the algorithm of Fig. 1 (c) by reducing the fast fluctuations of the pre-filtered phase noise estimate in each iteration. Such fast fluctuations, caused by high frequency components, do not adhere to the low-pass nature of the phase noise. Therefore, the low-pass filter allows a better estimate of the phase noise.

As mentioned in the previous subsection, the low-pass filter adjust to the spectral shape of the phase noise. This spectral shape can be characterized by two parameters: the cutoff frequency (f_c) and the decay slope (m_f). These two parameters can be obtained from the preamble of the transmitted signal. Hence, the low-pass filter can be designed with a flat amplitude until f_c and a linear logarithmic decay from f_c with a slope value defined by m_f.

The pre-filtered phase noise estimate yields less accurate results at the first iterations due to the higher number of errors in the demodulation process and, thus, this estimate contains more fluctuations at high frequencies. Hence, the strictness of the filter has to decrease progressively for these high frequencies in each iteration. This strictness can be translated to the m_f value of the filter. Thus, m_f decreases with the number of iterations, implementing an adaptive low-pass filter in the presented algorithm. In this way, its performance can be enhanced and optimized.

Fig. 2 shows an adaptive low-pass filter example. This is composed of six filters with decreasing m_f values. Therefore, the more attenuation in the filter, the earlier iteration we are considering. The f_c value of this example is 0.5 MHz. From this frequency point until half the sampling frequency of the signal (0.12 GHz, in this case), the attenuation of the adaptive filter decreases proportionally from 80 to 10 dB. The related values of m_f (in dB/decade) to these attenuation values are shown in the inset of Fig. 2. Comparing with the algorithms

proposed in [19], [21], [22], the novelty of this algorithm lies in the adaptability of the inserted low-pass filter for each iteration to improve performance. Furthermore, since the characteristics of the used low-pass filter implies a big impact in the phase noise estimate [21], the guidelines to design the low-pass filter have been shown in this section.

C. Complexity and latency analysis

The complexity associated to the digital signal processing (DSP) is a decisive factor in mobile communications. The additional complexity factor (C_F) of the proposed algorithm with respect to the standard OFDM receiver can be calculated approximately as:

$$C_F = \frac{I \cdot N \cdot (7.75 + 2.5 \cdot \log_2(N))}{N \cdot (2.5 + \log_2(N))} \quad (1)$$

with N being the number of subcarriers to process in the FFT and IFFT blocks, where I denotes the total number of iterations in the algorithm. The numerator of the Eq. (1) refers to the total number of complex multiplications of the algorithm, whereas the denominator corresponds to the number of complex multiplications of the standard OFDM receiver (see green blocks in Fig. 1 (c)). Thereby, the additional complexity factor of the algorithm is roughly 2.5 per iteration. This rate is valid for most of N values since Eq. (1) is linear in terms of N. This shows that there is a trade-off between complexity and performance, since yield increases as shown in Section V. Since the power consumption is highly related to the complexity of the algorithm in terms of number of multiplications, the additional power consumption, added by the algorithm, is also approximately 2.5 times more than the conventional OFDM receiver.

Assuming a pipeline process where all the blocks of the algorithm can be performed in parallel, the additional latency factor in terms of multiplication latency is:

$$L_F = \frac{I \cdot (18 + 4 \cdot \log_2(N))}{4 + \log_2(N))} \quad (2)$$

Eq. (2) has been calculated considering that most of the multiplications of the algorithm can be performed in parallel. However, the FFT and IFFT processes require a certain number of stages that cannot be realized in parallel. The $\log_2(N)$ terms of Eq. (2) correspond to the delay of these stages. In addition, the numerator of this equation refers to the multiplication latencies of the algorithm, whereas the denominator corresponds to the number of multiplication latencies of the classical OFDM receiver. The additional latency factor (L_F) of the proposed algorithm can be approximated to 4 per iteration. The main reason of this high latency factor value is the use of a high-selectivity frequency filter. Since the proposed algorithm increases the final latency of the link in terms of tens of microseconds per iteration and the final latency of the link is in terms of hundreds of milliseconds, the increased latency factor of the algorithm is not critical respecting the final latency [23].

Finally it should be noted that in terms of system or standardization complexity, this algorithm is not expected to cause any interoperability issues. As it is entirely local to the receiver and does not require adaptation of the modulation format or signaling, it can be introduced by any equipment/phone manufacturer in their receiver to improve performance in the presence of phase noise, e.g., as a special variant or differentiating feature.

III. Experimental Setup

The experimental setup used to study and analyze the phase noise in OFDM mm-wave ARoF systems is shown in Fig. 3 (a). First, an external cavity laser (ECL) generates the optical carrier at 1550 nm. Next, this optical carrier is modulated by a 25 GHz Mach–Zehnder modulator (MZM), biased in the null point, and driving with a sinusoid of 12.5 GHz generated by a vector signal generator (VSG). Therefore, two optical tones are produced with a frequency separation of 25 GHz. The spectrum of these two tones can be observed in Fig. 3 (a.1).The optical two-tone signal is boosted by an erbium-doped fiber amplifier (EDFA). Next, the two tones are separated by a wavelength selective switch (WSS). The left tone is processed in the lower branch (see Fig. 3 (a.2)), and the right tone in the upper branch (see Fig. 3 (a.3)).

One tone is modulated by a second 10 GHz MZM, biased in the quadrature point, with the OFDM signal. This OFDM signal is produced by an arbitrary waveform generator (AWG) with a sampling rate of 12 GSa/s. In the lower branch, the second tone is delayed with respect to the upper tone. This delay is performed by patch cords with different lengths. Thus, the phase noise of the system can be increased gradually by adding longer patch cords. Then, the modulated and delayed tones are recombined in an optical coupler. The optical spectrum of the combined signal is shown in Fig. 3 (a.4). A polarization controller (PC) is added to the lower branch in order to match the polarization of two branches.

The recombined optical tones beat on a 40 GHz photodiode (PD) producing a modulated RF signal at 26 GHz. The spectrum of this modulated RF signal is represented in Fig. 3 (a.5). In this figure, both the OFDM double sideband with an intermediate frequency (IF) of 1 GHz and the 25 GHz carrier can be observed. Thereby, one OFDM sideband is generated at 24 GHz, whereas the other is at 26 GHz. Considering the wireless link to be implemented in this system, an RF filter, whose task consists of removing the RF carrier at 25 GHz and one of the OFDM sidebands, should be necessary to add before the antenna. Then, the electrical signal is boosted by a 30 dB medium power amplifier (MPA) with 18 to 40 GHz of bandwidth. Next, the boosted signal is mixed with a sinusoid of 23 GHz generated by a second VSG. Consequently, the electrical signal is down-converted to a second IF of 2 GHz. Therefore, the total IF is 3 GHz. Last, the IF signal is sampled and stored by a digital phosphor oscilloscope (DPO) with 12.5 GSa/s of sampling rate.

In the tables of Fig. 3 (b), the values of the measured optical and electrical power values for certain points of the experimental setup are shown. The optical power value with index seven is marked with an asterisk because it depends on the length of the used patch cord. Moreover, the transmitter block diagram of the OFDM DSP is detailed in Fig. 3 (c). First,

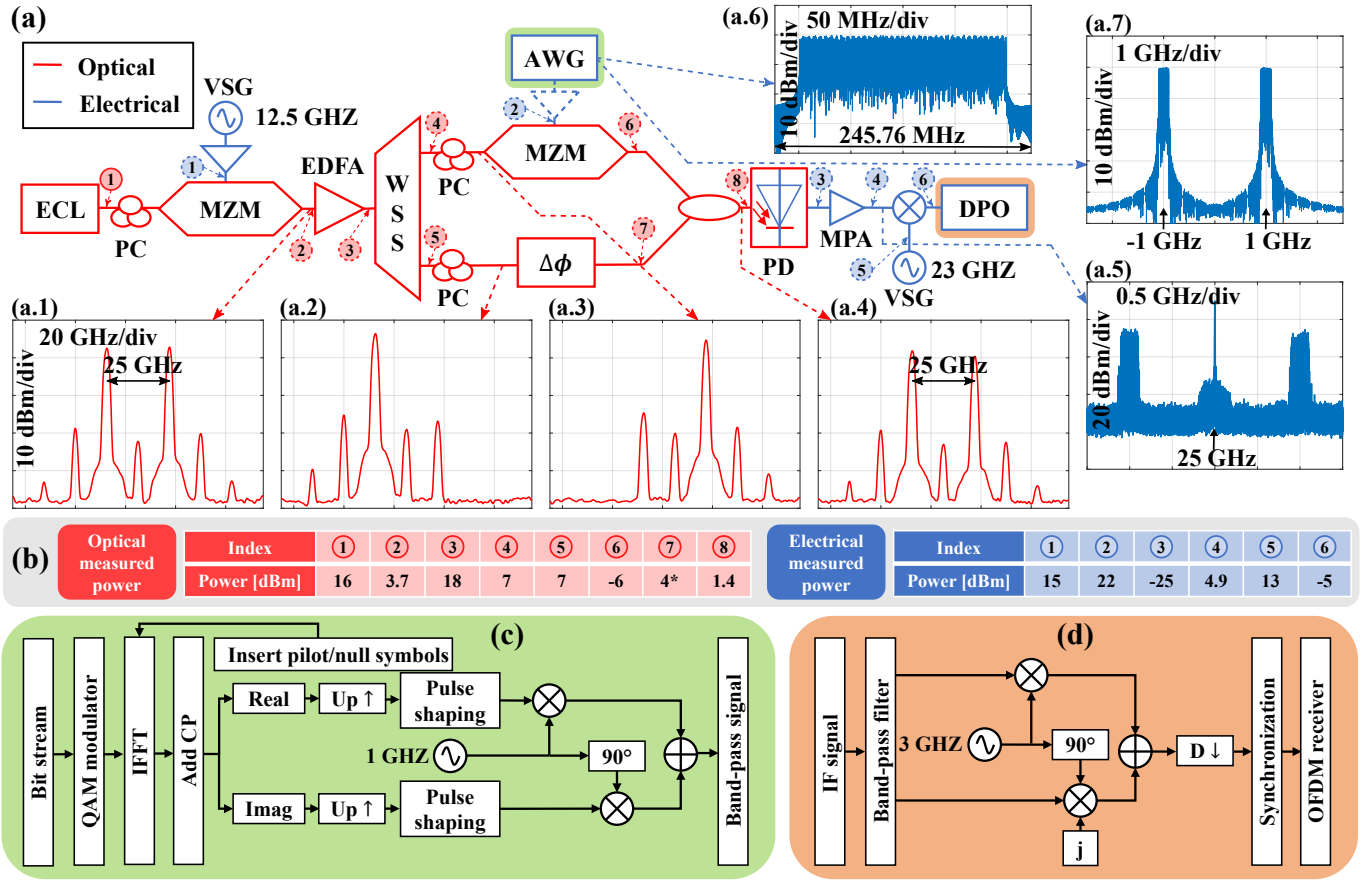

Figure 3. Experimental testbed: (a) scheme of the setup, (b) tables with the measured power values in several points of the experimental setup, (c) block diagram of the DSP in the transmitter, (d) and block diagram of the DSP in the receiver.

a pseudorandom bit stream is generated. Then, these bits are modulated according to a quadrature amplitude modulation (QAM), producing complex QAM symbols. These symbols correspond to the data subcarriers of the OFDM signal. After this process, pilot symbols are equally distributed between the generated data subcarriers. Moreover, null subcarriers are added in the edges of the OFDM band, achieving lower out-of-band (OOB) emissions. Next, an IFFT is performed and CP is added to the time-domain OFDM signal. The spectrum of the OFDM signal after this process is shown in Fig. 3 (a.6). Then, the real and imaginary parts are divided and upsampled. A pulse shaping process is carried out in the real and imaginary branches independently. Next, the real and imaginary signals are multiplied by a cosine and sine of 1 GHz, respectively. Last, the signals from both branches are combined, producing an OFDM band-pass signal with an IF of 1 GHz (see Fig. 3 (a.7)).

The receiver DSP process is shown in Fig. 3 (d). The IF signal sampled in the DPO is filtered by a band-pass filter. Then, the filtered signal is down-converted to baseband by multiplying with a cosine and sine of 3 GHz (total IF) for the real and imaginary parts, respectively. Next, the complex baseband signal is downsampled and synchronized. Finally, the OFDM receiver of Fig. 1 (c) is used. It is important to mention that all DSP processes are offline. Different OFDM numerologies are transmitted and compared using this setup. All these OFDM configurations have the same bandwidth (245.76 MHz) and bit rate (677.18 Mbps), getting an equal spectral efficiency value (2.76 bit/s/Hz) and, thus, a fair comparison is achieved. The common parameters for all the used OFDM configurations are the next: 16-QAM as modulation; the 80.5% of the total subcarriers are active; and one pilot inserted on every 12th subcarrier. The rest of the parameters are presented in Table I: subcarrier spacing (Δf), total number of subcarriers (N), and CP period (T_{cp}).

Table I
OFDM CONFIGURATION PARAMETERS.

Config.	1	2	3	4	5
Δf [KHz]	15	30	60	120	240
N	2^{14}	2^{13}	2^{12}	2^{11}	2^{10}
T_{cp} [µs]	4.8	2.4	1.2	0.6	0.3

IV. PHASE NOISE ANALYSIS IN ARoF SYSTEMS

This section is focused on analyzing, estimating and simulating the phase noise level for different time delay values in the setup of Fig. 3 (a). The power spectral density (PSD) of the phase noise is measured before the DPO by an electrical spectrum analyzer (ESA) for different lengths of the patch

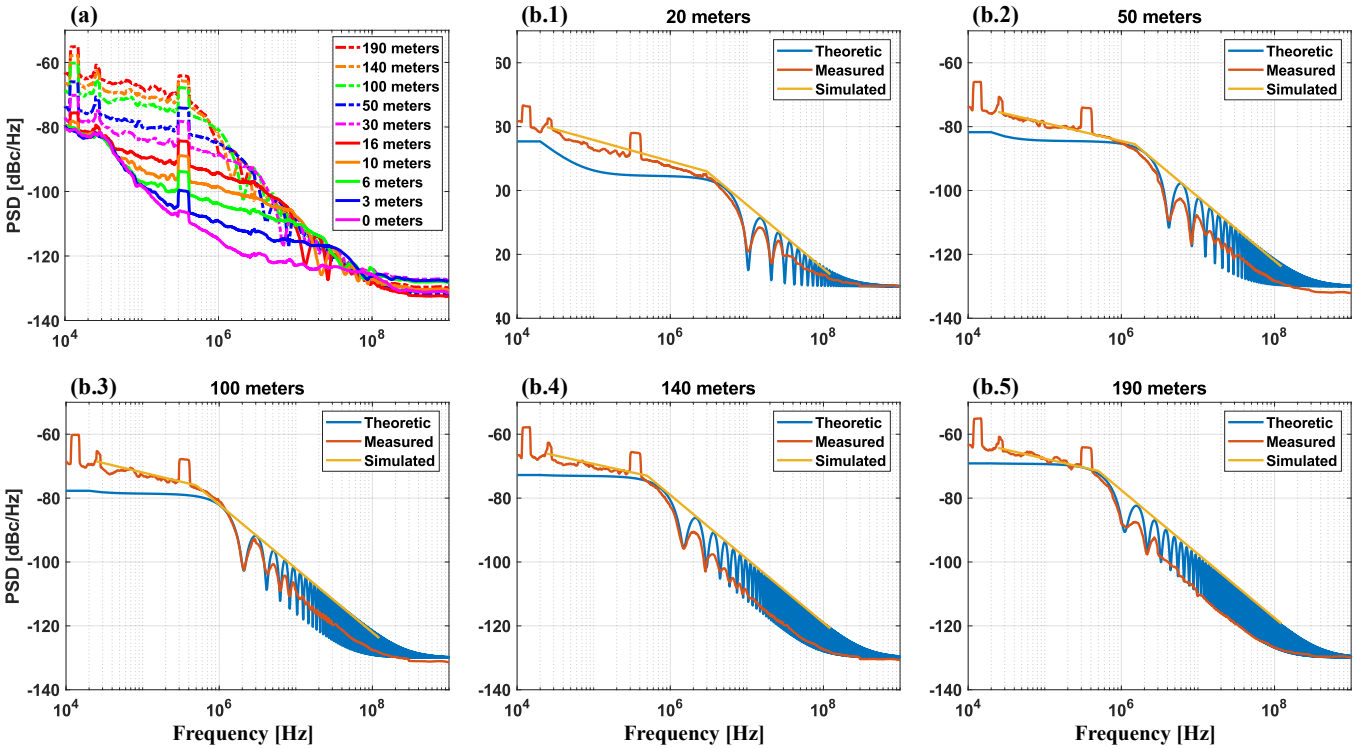

Figure 4. (a) PSD of the phase noise measured before the DPO for different path delays. (b) Theoretic, measured, and simulated PSD of the phase noise for different path lengths: 20 m (b.1), 50 m (b.2), 100 m (b.3), 140 (b.4), and 190 m (b.5).

cord. These PSD measures are shown in Fig. 4 (a). The PSD of the phase noise is measured for path length differences between 0 m and 190 m. The delay corresponding to these path lengths can be calculated as:

$$\Delta\tau = \frac{n \cdot \Delta L}{c}, \tag{3}$$

where n is the refractive index of the fiber, ΔL denotes the length of the patch cord, with c being the speed of light in vacuum. In Fig. 4 (a), it can be noticed that the PSD level of the phase noise increases with the path length, 0 m being the condition with minimum phase noise and 190 m the maximum one. This phase noise increment is due to the decorrelation between two tones as distance increases. Furthermore, the phase noise of the 0 m case is not zero because the AWG and VSGs form phase noise to the system [24]. The phase noise added by the AWG and the VSGs are present in all the cases of Fig. 4 (a). Moreover, from a 10 m-path length, the phase noise PSD shows a fading pattern because the two branches of the setup form an interferometric structure. As a common remarkable feature in all the phase noise measures, the PSD level starts to decrease with higher decay slope from 0.5 MHz of frequency. This cutoff frequency is crucial for the design of the adaptive low-pass filter of the proposed algorithm presented in Section II. The PSDs of the phase noise for these path delays can be estimated as [24]:

$$S(f) = \left\{ \left(\exp\left(B_{OP}\left|\tau_d\right|\right) - B_{OP}\frac{\sin(2\pi f\left|\tau_d\right|)}{2\pi f} - \cos(2\pi f\left|\tau_d\right|) \right) \times \frac{2B_{OP}\exp\left(-B_{OP}\left|\tau_d\right|\right)}{(\sqrt{2}B_{OP})^2 + (2\pi f)^2} \right\} * \frac{2B_{LO}}{(2B_{LO})^2 + (2\pi f)^2} \tag{4}$$

where B_{OP} is the angular full linewidth at half maximum (FWHM) of the optical laser, τ_d is the delay difference between the two branches, and B_{LO} is the FWHM of the first VSG. Both the theoretical calculation and actual measurements of the phase noise PSD are shown in Fig. 4 (b) for the different path lengths indicated above. It can be observed that the theoretical fading pattern matches the measured PSD one. However, the amplitudes of these PSDs do not coincide completely. This fact is due to the resolution of the ESA used to obtain the PSD measures not being high enough. Furthermore, the PSD of the phase noise used in the simulations is also depicted in Fig. 4 (b). The simulated phase noise approximates the theoretical one through three points.

V. Results and Discussion

In this section, the simulation and experimental results are discussed and analyzed. The OFDM configurations of Table I are evaluated under different path delays: 20 m, 50 m, 100 m, 140 m, and 190 m. The error vector magnitude (EVM) values in percent for the different OFDM configurations and different phase noise conditions are shown in Fig. 5. The standard

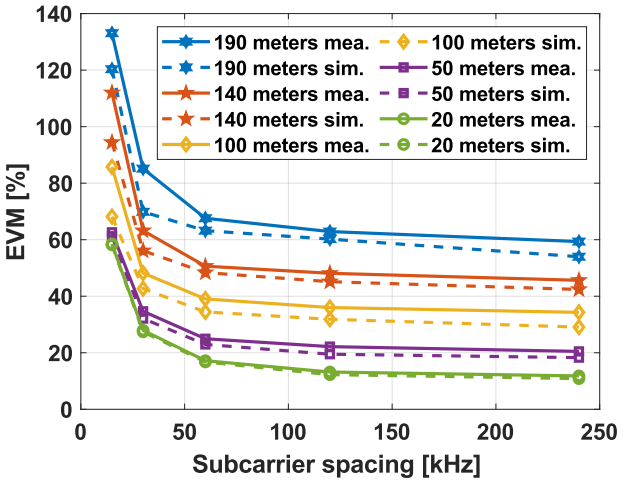

Figure 5. Simulated (solid lines) and experimental (dashed lines) EVM as function of the subcarrier spacing for different path delays.

OFDM receiver (green blocks in Fig. 1 (c)) is utilized to obtain the EVM values of this graph. The simulation results are also illustrated in Fig. 5. The simulated channel only includes phase noise (according to the simulated PSD of the phase noise in Fig. 4 (b)) and AWGN, reproducing the same signal-to-noise ratio (SNR) level as in the experimental setup (26 dB). It can be observed in Fig. 5 that the simulation and experimental results match well.

Examining Fig. 5, the EVM follows a decreasing exponential curve as OFDM subcarrier spacing increases. This decay of the EVM is due to the fact that the ICI induced by the phase noise is proportional to the OFDM subcarrier spacing as explained in Section II. Moreover, as the phase noise level increases with the path length, the EVM values of the standard OFDM receiver do too. For most cases, the EVM values shown in Fig. 5 are considerably high for a 16-QAM constellation. Therefore, a method to mitigate the phase noise is truly required to establish a proper communication quality.

Fig. 6 shows the EVM values for the OFDM configurations in Table I and for different path lengths by employing the algorithm introduced in Section II. These EVM values are presented as a function of the concrete number of iterations of the proposed algorithm. In addition, the constellations of the processed signal using two iterations are also displayed for the different path delays. The EVM threshold of 12.5% for 16-QAM, determined by the 3GPP [9], is also indicated.

As the PSD level seen in Fig. 4 (b) starts to decrease from, approximately 0.5 MHz in a more remarkable manner, the used adaptive low-pass filter shapes for six iterations are the same that shown in Fig. 2. For the remaining iterations, the attenuation of the filters is as linear steps between 80 and 10 dB. For instance, for three iterations, the attenuation values for the used filter are 80, 45, and 10 dB, respectively. Furthermore, this filtering process is performed in the frequency-domain to configure and approximate in a more accurate way the desired frequency shape. Therefore, this filtering block implies an additional FFT and IFFT stages. It is also worth mentioning that the equalizer block considers to be flat the amplitude of the estimated channel. In this respect, since the channel of the experimental setup does not present significant fadings in the frequency domain, the performance of the results enhances.

Table II
NUMBER OF ITERATIONS TO REACH 5G EVM REQUIREMENTS FOR 16-QAM.

Δf [KHz]	15	30	60	120	240
20 m	2	2	1	1	0
50 m	3	2	1	1	1
100 m	3	2	2	2	2
140 m	3	3	3	3	3
190 m	3	3	3	3	4

Observing Fig. 6, it can be noticed that the EVM threshold of 12.5% for 16-QAM in 5G is achieved for all OFDM configurations and all the different phase noise levels. The required number of iterations to achieve the 5G threshold for all the different cases is shown in Table II. This shows that the required number of iterations of the algorithm increases as phase noise increases. At this point, we must highlight that the number of iterations increases the complexity of the system. Hence, more complexity in the receiver is demanded when higher phase noise levels are mitigated. Furthermore, since the ICI induced by the phase noise decreases with the subcarrier spacing, the required number of iterations of the algorithm, to satisfy EVM values lower than 12.5%, is lower for higher subcarrier spacings. However, for 140 m of path length, the needed iterations maintain constant and, for the 190 m case, 240 kHz of subcarrier spacing presents the highest value of iterations. This fact is because higher subcarrier spacing configurations use less number of pilot tones and, thus, the equalization process contains more noise in higher path lengths than in lower subcarrier spacing values. Therefore, due to the degradation in the equalizer, high subcarrier spacing values, as 240 kHz, perform worse in channels with high phase noise level.

Furthermore, the OFDM receiver signal suffers frequency offset (FO) due to the frequency mismatch between the transmitter and receiver oscillators. In the experimental setup of Fig. 3 (a), the measured FO value is 20 kHz. Therefore, the proposed algorithm can handle the degradation of the signal induced by FO. However, since the EVM increases as the FO increases, more iterations are needed for higher FO values to achieve the 5G requirements. Then, when large FOs are present, it is common to have a dedicated coarse FO estimation and compensation before the OFDM processing [25] and the same should be applied here. Thereby, the number of iterations of the algorithm do not need to increase when FO increases.

VI. CONCLUSIONS

This article discussed the relevance of studying and compensating phase noise in mm-wave ARoF systems for 5G. A novel and efficient algorithm to mitigate phase noise in the OFDM receiver was presented, its complexity analyzed and performance simulated. Moreover, a mm-wave ARoF setup at 25 GHz was implemented to experimentally analyze the impact of phase noise on 5G NR OFDM signals. The configuration

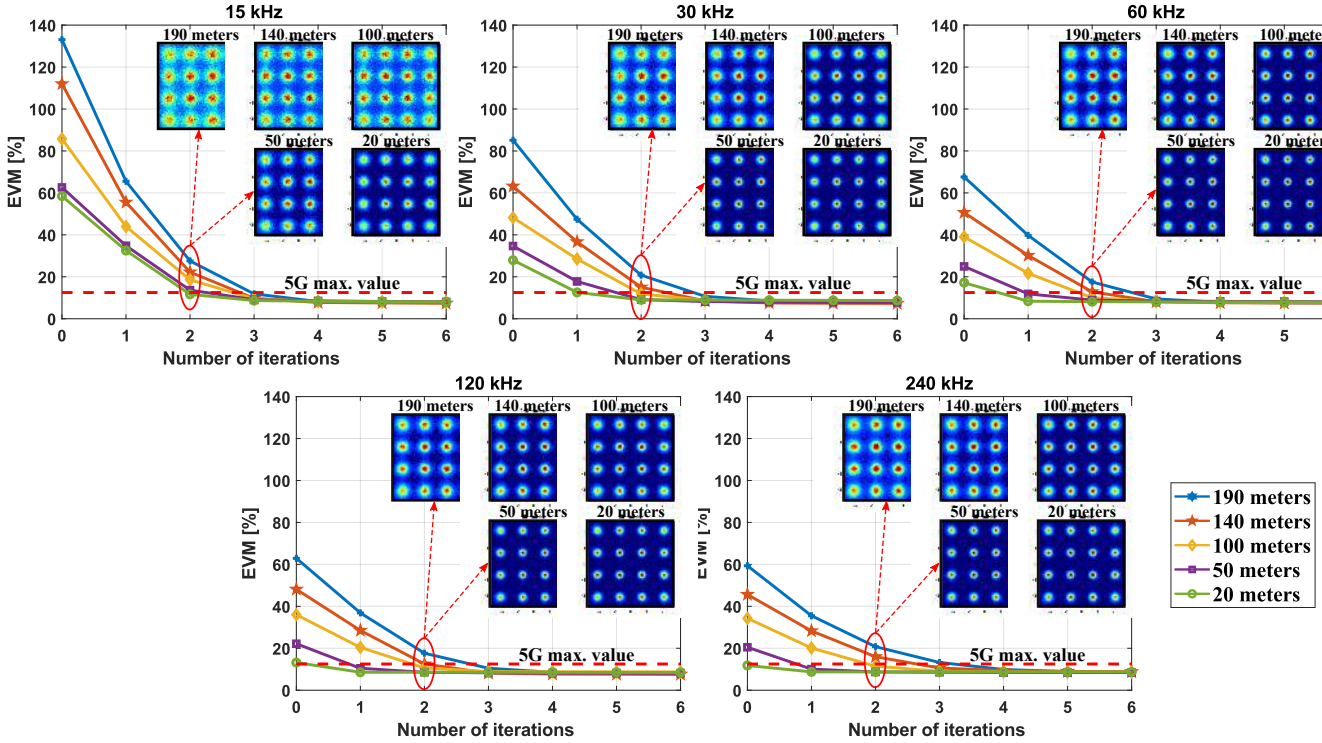

Figure 6. EVM as a function of the number of iteration in the proposed OFDM receiver for different subcarrier spacings and under different phase noise levels .

of this setup allowed to gradually scale the phase noise level in the received signal.

OFDM signals with different subcarrier spacings, according to the 5G NR numerology, were evaluated in the experimental setup under different phase noise conditions. First, the standard OFDM receiver was utilized to process the received OFDM signals. The results of this process in terms of EVM were shown and matched with simulations. Then, the proposed algorithm was used to compensate the degradation due to phase noise and to decode the received signal, showing substantial improvements in performance and reduction of EVM, especially at high levels of phase noise. As a result, the proposed ARoF system can reach the EVM requirements posed by 5G standards even in the presence of substantially higher phase noise levels than acceptable with a standard OFDM receiver.

The experimental results validate the proposed algorithm under different phase noise conditions and with different OFDM subcarrier spacings. By providing an efficient algorithm for compensation of phase noise in mm-wave ARoF systems employing OFDM signals, this work proves the viability of mm-wave ARoF links for 5G and beyond.

REFERENCES

[1] D. Konstantinou *et al.*, "5G RAN architecture based on analog radio-over-fiber fronthaul over UDWDM-PON and phased array fed reflector antennas," *Optics Communications*, vol. 454, pp. 0030–4018, Jan. 2020.

[2] W. H. Chin, Z. Fan, and R. Haines, "Emerging technologies and research challenges for 5G wireless networks," *IEEE Wirel. Commun.*, vol. 21, no. 2, pp. 106–112, Apr. 2014.

[3] M. R. Akdeniz *et al.*, "Millimeter Wave Channel Modeling and Cellular Capacity Evaluation," *IEEE J. Sel. Areas Commun.*, vol. 32, no. 6, pp. 1164–1179, Jun. 2014.

[4] J. Brenes *et al.*, "Network slicing architecture for SDM and analog-radio-over-fiber-based 5G fronthaul networks," *J. Opt. Commun. Netw.*, vol. 12, no. 4, pp. B33–B43, Apr. 2020.

[5] S. Rommel *et al.*, "Towards a scaleable 5G fronthaul: Analog radio-over-fiber and space division multiplexing," *J. Light. Technol.*, vol. 38, no. 19, pp. 5412–5422, 2020.

[6] S. Rommel, D. Perez-Galacho, J. M. Fabrega, R. Muñoz, S. Sales, and I. Tafur Monroy, "High-Capacity 5G Fronthaul Networks Based on Optical Space Division Multiplexing," *IEEE Trans. Broadcast.*, vol. 65, no. 2, pp. 434–443, Jun. 2019.

[7] L. C. P. Cavalcante, S. Rommel, R. Dinis, L. G. Q. S. Junior, L. F. Q. Silveira, and I. T. Monroy, "Performance Evaluation of Wavelet-Coded OFDM on a 4.9 Gb/s W-Band Radio-Over-Fiber Link," *J. Lightwave Technol.*, vol. 35, no. 14, pp. 2803–2809, Jul. 2017.

[8] J. A. Altabas *et al.*, "Nonorthogonal Multiple Access and Carrierless Amplitude Phase Modulation for Flexible Multiuser Provisioning in 5G Mobile Networks," *J. Lightwave Technol.*, vol. 35, no. 24, pp. 5456–5463, Dec. 2017.

[9] 3GPP, *FG IMT-2020: User Equipment (UE) radio transmission and reception; Part 2: Range 2 Standalone. 3GPP TS 38.101-2, version 16.3.1, Release 16*, 2020.

[10] J. P. Santacruz, S. Rommel, U. Johannsen, A. Jurado-Navas, and I. T. Monroy, "Candidate Waveforms for ARoF in Beyond 5G," *Appl. Sci.*, vol. 10, 3891, Jun. 2020.

[11] J. P. Santacruz, A. Morales, S. Rommel, U. Johannsen, A. Jurado-Navas, and I. T. Monroy, "Experimental Assessment of Modulation Formats for Beyond 5G mm-Wave ARoF Systems," 2020, accepted.

[12] A. Delmade *et al.*, "OFDM Baud Rate Limitations in an Optical Heterodyne Analog Fronthaul Link using Unlocked Fibre Lasers," in *International Topical Meeting on Microwave Photonics (MWP)*, Nov. 2019, pp. 1–4.

[13] E. P. Martin *et al.*, "25-Gb/s OFDM 60-GHz Radio Over Fiber System Based on a Gain Switched Laser," *J. Light. Technol.*, vol. 33, no. 8, pp. 1635–1643, Jan. 2015.

[14] T. Shao *et al.*, "Chromatic Dispersion-Induced Optical Phase Decorrelation in a 60 GHz OFDM-RoF System," *IEEE Photon. Technol. Lett.*, vol. 26, no. 20, pp. 2016–2019, Aug. 2014.

[15] C. Wei, C. Lin, H. Huang, W. Liang, and S. Chi, "Estimation and Suppression of Dispersion-Induced Phase Noise in W-band Direct-Detection OFDM Radio-Over-Fiber Systems," *J. Light. Technol.*, vol. 32, no. 20, pp. 3874–3884, May 2014.
[16] H.-T. Huang, W.-L. Liang, C.-C. Wei, C.-T. Lin, and S. Chi, "150-km 103-GHz Direct-Detection OFDM-RoF System Employing Pilot-aided Phase Noise Suppression," in *Optical Fiber Communication Conference*. San Francisco, CA, USA: Optical Society of America, Mar. 2014, p. M2D.6.
[17] C. Browning, E. P. Martin, A. Farhang, and L. P. Barry, "60 GHz 5G Radio-Over-Fiber Using UF-OFDM With Optical Heterodyning," *IEEE Photon. Technol. Lett.*, vol. 29, no. 23, pp. 2059–2062, Oct. 2017.
[18] C. Browning *et al.*, "Gain-Switched Optical Frequency Combs for Future Mobile Radio-Over-Fiber Millimeter-Wave Systems," *J. Light. Technol.*, vol. 36, no. 19, pp. 4602–4610, May 2018.
[19] V. Syrjälä and M. Valkama, "Flexible adjacent channel interference and phase noise suppression in energy-efficient OFDMA receivers," in *Proc. IEEE 17th CAMAD*, Barcelona, Spain, Oct. 2012, pp. 221–225.
[20] A. Demir, A. Mehrotra, and J. Roychowdhury, "Phase noise in oscillators: a unifying theory and numerical methods for characterization," *IEEE Trans. Circuits Syst. I: Fundamental Theory and Applications*, vol. 47, no. 5, pp. 655–674, May 2000.
[21] V. Syrjala and M. Valkama, "Receiver DSP for OFDM Systems Impaired by Transmitter and Receiver Phase Noise," in *Proc. IEEE International Conference on Communications (ICC)*, Kyoto, Japan, Jul. 2011, pp. 1–6.
[22] C.-T. Lin, C.-C. Wei, and M.-I. Chao, "Phase noise suppression of optical OFDM signals in 60-GHz RoF transmission system," *Opt. Express*, vol. 19, no. 11, pp. 10 423–10 428, May. 2011.
[23] I. Parvez, A. Rahmati, I. Guvenc, A. I. Sarwat, and H. Dai, "A Survey on Low Latency Towards 5G: RAN, Core Network and Caching Solutions," *IEEE Commun. Surv. Tutor.*, vol. 20, no. 4, pp. 3098–3130, May 2018.
[24] T. Shao, F. Paresys, G. Maury, Y. L. Guennec, and B. Cabon, "Investigation on the Phase Noise and EVM of Digitally Modulated Millimeter Wave Signal in WDM Optical Heterodyning system," *J. Light. Technol.*, vol. 30, no. 6, pp. 876–885, Jan. 2012.
[25] T. M. Schmidl and D. C. Cox, "Robust frequency and timing synchronization for OFDM," *IEEE Trans. on Commun.*, vol. 45, no. 12, pp. 1613–1621, Dec. 1997.

Javier Pérez Santacruz received his BSc degree in Telecommunication Engineering from the University of Málaga (Spain) in 2016 and his double MSc degree in Telecommunications Engineering and Telematic and Telecommunication Networks from the University of Málaga (Spain) in 2018. He completed his thesis entitled "Simulator of a bandwidth modem for underwater acoustic channels".

Since 2018 he is with Eindhoven University of Technology as a Ph.D. candidate. His research is focused on modulation formats and digital signal processing in millimeter wave (mm-Wave) analog-radio-over-fiber (ARoF) systems for 5G and beyond. Moreover, he is member of the ITN project 5G STEP FORWARD.

Simon Rommel (S'15–M'18) obtained his B.Sc. degree from the University of Stuttgart, Germany in 2011 and in 2014 obtained M.Sc. degrees in Photonic Networks Engineering from Aston University, Birmingham, UK and Scuola Superiore Sant'Anna, Pisa, Italy. He completed his Ph.D. in 2017 at the Technical University of Denmark, Kongens Lyngby, Denmark with research focused on photonic-wireless convergence and millimeter-wave radio-over-fiber links. In 2017 he visited the National Institute of Information and Communications Technology, Koganei, Tokyo, Japan for a research stay.

Since 2017 he is with Eindhoven University of Technology as a post-doctoral researcher, continuing his work photonic and radio frequency technologies with a strong focus on implementations for 5G. His research interests include the fields of fiber-optic and wireless communications and the associated digital signal processing. He has contributed to multiple national and European research projects, incl. H2020 blueSPACE as technical manager.

Dr. Rommel is a member of Institute of Electrical and Electronics Engineers (IEEE), The Optical Society (OSA), the Institution of Engineering and Technology (IET) and the Verband der Elektrotechnik Elektronik Informationstechnik e.V (VDE).

Ulf Johannsen obtained his Dipl.-Ing. degree from Hamburg University of Technology (TUHH), Germany, in 2009 and his Ph.D. degree from Eindhoven University of Technology (TU/e), the Netherlands, in 2013. In the same year he started as Senior Systems Engineer at ATLAS ELEKTRONIK GmbH in Bremen, Germany. Here, he worked as system designer and engineering manager on autonomous underwater vehicle (AUV) systems with sonar payloads. His responsibilities included the specification and architecting of the entire systems as well as the lead of multi-disciplinary development teams in order to meet those specifications within time and budget. Since 2016 he is assistant professor with the Electromagnetics group at TU/e. His research focus lies on (sub-)millimetre-wave antenna systems for various applications. Moreover, he leads the Ultra-High-Data-Rate programme within TU/e's Centre for Wireless Technology. Dr. Johannsen is the chairperson of the IEEE Benelux joint AP/MTT chapter.

Antonio Jurado-Navas obtained his Ph.D. degree (2009) in Telecommunication Engineering from the University of Málaga (Spain). From 2002 to 2004 he worked as a consultant at Vodafone-Spain. He was the recipient of a Spanish Ministry of Education and Science scholarship (2004-2008) From 2009 to 2011, he was with the Department of Communications Engineering (Ingeniería de Comunicaciones) at the University of Málaga as a postdoctoral researcher. In 2011, he became an Assistant Professor in the same department. From 2012 to 2015, he was with Ericsson Spain, where he was working on geolocation tools for mobile networks. From 2015 to 2017, he was a Marie-Curie fellow at the Technical University of Denmark (Kongens Lyngby, Denmark). In 2017, Dr. Jurado-Navas joined Technical University of Eindhoven to work for the Electro-Optical Communications (ECO) group as an invited researcher. Since 2018, he is an Associate Professor with the Communication Engineering Department, Universidad de Málaga. His research interests span a diverse set of topics in the wide areas of communication theory and wireless communications: free-space optical communications, stochastic processes, wireless channel modeling, OCDMA, physical layer security, adaptive optics, and efficient transmission techniques.

Idelfonso Tafur Monroy is since July 2017, Professor in photonic Terahertz systems at the department of Electrical Engineering of the Eindhoven University of Technology, and since November 2018 director of the Photonic Integration Technology Center (PITC).

He coordinates the 5G PPP BLUESPACE project on technologies for 5G wireless systems and the ITN CELTA project with 15 PhD students working convergence of electronics and photonics technologies for applications such as THz communications, sensing and imaging.

His research interests are in the area photonics technologies for Terahertz systems, converged electronic-photonic integrated circuits for applications in secure communications, sensing and computing. He is co-author of over 500 journal and conference papers and has graduated 22 PhD students. He is co-founder of the start-up Bifrost Communications on optical fiber access solutions.

Idelfonso Tafur started his academic career in the Kharkov Polytechnic Institute in Ukraine, he received a M.Sc degree from the Bonch-Bruevitch Institute of Communications, St. Petersburg, Russia, holds a Technology Licentiate degree in telecommunications theory from the Royal Institute of Technology, Stockholm, Sweden, and a PhD degree from the Eindhoven University of Technology.

He has been Professor in photonics communication technologies at Technical University of Denmark, guest Professor at the Beijing University of Post and Telecommunications, visiting scientist at the University of California at Berkeley and Fellowship Professor at the ITMO University in St Petersburg Russia, and is a senior member of IEEE.